

Spatial patterns of brain amyloid- β burden and atrophy rate associations in mild cognitive impairment

Duygu Tosun,¹ Norbert Schuff,^{1,2,3} Chester A. Mathis,⁴ William Jagust,⁵ Michael W. Weiner^{1,2,3} and Alzheimer's Disease Neuroimaging Initiative*

1 Center for Imaging of Neurodegenerative Diseases, San Francisco VA Medical Centre, San Francisco, CA, USA

2 Department of Radiology, University of California, San Francisco, CA, USA

3 Department of Neurology, University of California, San Francisco, CA, USA

4 Department of Radiology, PET Facility, University of Pittsburgh, Pittsburgh, PA, USA

5 Helen Wills Neuroscience Institute and School of Public Health, University of California Berkeley, CA, USA

*Data used in the preparation of this article were obtained from the Alzheimer's Disease Neuroimaging Initiative (ADNI) database (www.loni.ucla.edu/ADNI). As such, the investigators within the ADNI contributed to the design and implementation of ADNI and/or provided data but did not participate in analysis or writing of this report. Complete listing of ADNI investigators is available at http://www.loni.ucla.edu/ADNI/Collaboration/ADNI_Authorship_list.pdf

Correspondence to: Duygu Tosun, Ph.D.,
Center for Imaging Neurodegenerative Diseases,
Department of Veterans Affairs Medical Centre,
4150 Clement Street,
Building 13, 114 M,
San Francisco, CA, 94121, USA
E-mail: duygu.tosun@ucsf.edu

Amyloid- β accumulation in the brain is thought to be one of the earliest events in Alzheimer's disease, possibly leading to synaptic dysfunction, neurodegeneration and cognitive/functional decline. The earliest detectable changes seen with neuroimaging appear to be amyloid- β accumulation detected by ¹¹C-labelled Pittsburgh compound B positron emission tomography imaging. However, some individuals tolerate high brain amyloid- β loads without developing symptoms, while others progressively decline, suggesting that events in the brain downstream from amyloid- β deposition, such as regional brain atrophy rates, play an important role. The main purpose of this study was to understand the relationship between the regional distributions of increased amyloid- β and the regional distribution of increased brain atrophy rates in patients with mild cognitive impairment. To simultaneously capture the spatial distributions of amyloid- β and brain atrophy rates, we employed the statistical concept of parallel independent component analysis, an effective method for joint analysis of multimodal imaging data. Parallel independent component analysis identified significant relationships between two patterns of amyloid- β deposition and atrophy rates: (i) increased amyloid- β burden in the left precuneus/cuneus and medial-temporal regions was associated with increased brain atrophy rates in the left medial-temporal and parietal regions; and (ii) in contrast, increased amyloid- β burden in bilateral precuneus/cuneus and parietal regions was associated with increased brain atrophy rates in the right medial temporal regions. The spatial distribution of increased amyloid- β and the associated spatial distribution of increased brain atrophy rates embrace a characteristic pattern of brain structures known for a high vulnerability to Alzheimer's disease pathology, encouraging for the use of ¹¹C-labelled Pittsburgh compound B positron emission tomography measures as early indicators of Alzheimer's disease.

These results may begin to shed light on the mechanisms by which amyloid- β deposition leads to neurodegeneration and cognitive decline and the development of a more specific Alzheimer's disease-specific imaging signature for diagnosis and use of this knowledge in the development of new anti-therapies for Alzheimer's disease.

Keywords: MRI; ^{11}C -PiB PET; Alzheimer's disease; mild cognitive impairment; amyloid- β ; amyloid; brain atrophy rate; multimodal brain imaging

Abbreviations: ADNI = Alzheimer's Disease Neuroimaging Initiative; ^{11}C -PiB = ^{11}C -labelled Pittsburgh compound B

Introduction

The formation of amyloid plaques in the brain, mainly consisting of insoluble amyloid- β protein fragments, is thought to be a major factor that leads to degradation of neurons and ultimately to the development of Alzheimer's disease (Braak and Braak, 1991). Amyloid- β plaques, together with neurofibrillary tangles, are also the hallmarks of a definite diagnosis of Alzheimer's disease at autopsy (Braak and Braak, 1991). The development of radioligands, such as the ^{11}C -labelled Pittsburgh compound B (^{11}C -PiB), which binds to amyloid- β plaques, has made it possible to study plaque accumulation in life using ^{11}C -PiB PET (Klunk *et al.*, 2004; Mintun, 2005; Price *et al.*, 2005; Lockhart, 2006; Nordberg, 2007, 2008). Several ^{11}C -PiB PET studies have demonstrated increased brain amyloid- β deposition in patients with Alzheimer's disease (Price *et al.*, 2005; Kempainen *et al.*, 2006; Edison *et al.*, 2007; Mikhno *et al.*, 2008; Frisoni *et al.*, 2009; Tolboom *et al.*, 2009b; Devanand *et al.*, 2010). A growing number of ^{11}C -PiB PET studies have also reported increased brain amyloid- β in subjects with mild cognitive impairment (Price *et al.*, 2005; Kempainen *et al.*, 2007; Pike *et al.*, 2007; Rowe *et al.*, 2007; Forsberg *et al.*, 2008; Tolboom *et al.*, 2009b), individuals who fall between normal ageing and dementia and who have an increased risk of developing Alzheimer's disease (Petersen *et al.*, 2009). Furthermore, studies of cognitively normal elderly subjects suggest that the presence of amyloid- β , as detected by ^{11}C -PiB PET, is associated with a risk of developing symptomatic Alzheimer's disease (Klunk *et al.*, 2004; Mintun *et al.*, 2006; Kempainen *et al.*, 2007; Morris *et al.*, 2009). These results have raised the possibility that ^{11}C -PiB PET may detect preclinical Alzheimer's disease when treatment intervention may be most effective. However, about 10–30% of cognitively normal elderly subjects have amyloid- β positive findings on ^{11}C -PiB PET images even without apparent cognitive deficits (Galvin *et al.*, 2005; Driscoll *et al.*, 2006; Mintun *et al.*, 2006; Pike *et al.*, 2007; Rowe *et al.*, 2007; Aizenstein *et al.*, 2008; Villemagne *et al.*, 2008). Whether cognitively normal subjects with high levels of ^{11}C -PiB binding will develop Alzheimer's disease later on is unknown. Furthermore, only about 50% of patients with mild cognitive impairment advance to Alzheimer's disease within a short period of time (Lopez *et al.*, 2007) although 60–65% of all patients diagnosed with mild cognitive impairment are PiB-positive. The observations that some individuals tolerate high brain amyloid- β loads without cognitive deficits, while others suffer cognitive decline and there is a wide range in the rate of decline, suggest amyloid- β plaques alone are not sufficient to cause cognitive impairment and accompanying

neurodegeneration. In this study, we aim to shed light on the role of amyloid- β in neurodegeneration by elucidating the relationship between regional amyloid- β retention and progression of regional brain atrophy in subjects with clinically established cognitive impairments. We chose subjects diagnosed with mild cognitive impairment to test whether or not such a relationship can be detected in mild stages of brain atrophy. Furthermore, to detect both spatially localized as well as spatially distributed effects of amyloid- β retention on the progression of regional brain atrophy we utilized novel multivariate statistical methods for image analysis.

Over the past few years, several imaging studies have assessed amyloid- β deposition and brain atrophy together across a wide range of cognitive impairments using MRI and ^{11}C -PiB PET (Archer *et al.*, 2006; Fotenos *et al.*, 2008; Jack *et al.*, 2008b; Mormino *et al.*, 2009; Bourgeat *et al.*, 2010; Chetelat *et al.*, 2010). While a study of a healthy elderly population reported no associations between amyloid- β burden and regional rate of brain volume decline in the preceding years (Driscoll *et al.*, 2010), other studies have found an association between amyloid- β levels and brain tissue atrophy and ventricular expansion at mild stages of cognitive deficits (Jack *et al.*, 2009; Chetelat *et al.*, 2010). Even in stages of advanced cognitive impairment (e.g. after conversion to Alzheimer's disease), discrepant findings regarding an association between amyloid- β levels and brain atrophy have been reported (Archer *et al.*, 2006; Chetelat *et al.*, 2010). Though several factors might have contributed to these mixed findings, two aspects that are crucial for a better understanding of amyloid- β and brain atrophy relations were not addressed. First, no previous imaging study has determined to what extent the increased regional amyloid- β aggregation relates to increased rates of regional brain atrophy. Second, and perhaps more importantly, no previous study has investigated to what extent the regional variations in amyloid- β aggregation relate to regional variations in increased rates of brain atrophy across brain structures.

The main purpose of this study was to understand the relationship between the regional distribution of amyloid- β burden and the regional pattern of brain atrophy rates in mild cognitive impairment. Specifically, we tested two hypotheses: (i) increased amyloid- β levels in mild cognitive impairment are associated with increased brain atrophy rates; and (ii) the spatial distribution of elevated amyloid- β in mild cognitive impairment is associated with a characteristic pattern of increased and spatially distributed atrophy rates across brain structures typically involved in Alzheimer's disease pathology, such as the medial temporal lobe,

precuneus and posterior cingulate cortices. Conventional image statistics based on region of interests or voxel-wise tests, such as statistical parametric mapping (Worsley *et al.*, 2004) are generally limited to studies of localized relationships, i.e. when amyloid- β deposition leads to brain atrophy at the same location, but are inadequate to capture spatially distributed relations across the brain. To overcome this limitation, we turned to the concept of parallel independent component analysis, an effective method for joint analysis of multimodality imaging data (Calhoun and Adali, 2009). Parallel independent component analysis identifies not only variations across both image modalities but also variations across brain regions by evaluating all regional distributions simultaneously, thereby taking intrinsic relationships between these distributions into consideration. Therefore, our findings should lead to deeper insight into the biology of the disease than methods that evaluate the modalities as well as each brain region separately.

Materials and methods

Participants

The 61 participants diagnosed with mild cognitive impairment in this study were recruited between 2005 and 2008 through the Alzheimer's Disease Neuroimaging Initiative (ADNI) from 56 centres in the USA and Canada (Table 1) (Petersen *et al.*, 2010). The ADNI was funded as a prospective, longitudinal study to identify biomarkers of early Alzheimer's disease for clinical trials, supported by the National Institute on Ageing (NIA), the National Institute of Biomedical Imaging and Bioengineering (NIBIB), the Food and Drug Administration (FDA), private pharmaceutical companies and non-profit organizations, as a 5-year public-private partnership. Written consent was obtained from all subjects participating in the study, and the study was approved by the institutional review board at each participating site. This study also complied with the Health Insurance Portability and Accountability Act guidelines.

The subjects with mild cognitive impairment were over the age of 55 years with memory complaints and memory difficulties that were verified by an informant, scored below the education adjusted cut-off on a baseline Logical Memory II subscale (Delayed Paragraph Recall) from the Wechsler Memory Scale—Revised (Wechsler, 1987), scored

between 24 and 30 on a baseline Mini-Mental State Exam (Folstein *et al.*, 1975), scored a 0.5 on the Clinical Dementia Rating scale (Morris, 1993), scored at least 0.5 on the Memory Box and scored ≤ 12 on the 17-item Hamilton Depression rating scale at the ADNI study screening. General cognition and functional performance of each participant was sufficiently preserved such that a diagnosis of Alzheimer's disease could not be made by the site physician at the time of the screening visit. Participants with any significant neurological disease other than suspected incipient Alzheimer's disease, such as Parkinson's disease, multi-infarct dementia, Huntington's disease, normal pressure hydrocephalus, brain tumour, progressive supranuclear palsy, seizure disorder, subdural haematoma, multiple sclerosis or history of significant head trauma followed by persistent neurological defaults or known structural brain abnormalities as well as subjects with baseline MRI scans with evidence of infection, infarction, or other focal lesions, and with multiple lacunes or lacunes in a critical memory structure were excluded from the study. Further details regarding inclusion and exclusion criteria can be found at www.adni-info.org.

^{11}C -labelled Pittsburgh compound B data

^{11}C -PiB PET imaging is a recent addition to the ADNI protocol. The ^{11}C -PiB PET imaging procedure is outlined by Klunk *et al.* (2004). All baseline ^{11}C -PiB standardized uptake value ratio images that were available at the time of the study were downloaded from the ADNI web site (www.loni.ucla.edu/ADNI/). A detailed description of the ^{11}C -PiB PET image acquisition can be found at www.adni-info.org and details of the computation of ^{11}C -PiB standardized uptake value ratio images can be found at http://www.loni.ucla.edu/ADNI/Data/ADNI_Data.shtml.

Briefly, ADNI ^{11}C -PiB PET images were collected at 14 ADNI sites on multiple PET instruments of differing resolutions. ^{11}C -PiB with minimum 90% radiochemical purity and minimum specific activity of 300 Ci/mmol was synthesized using one of two methods (Wilson *et al.*, 2004; Mathis *et al.*, 2007). Subjects were injected with 15 ± 1.5 mCi ^{11}C -PiB. Dynamic acquisition frames were obtained on a PET scanner as 4×5 -min frames from 50–70 min after injection. Individual frames of the ^{11}C -PiB PET dynamic series were realigned if motion was detected and then a mean image was created in the native imaging space. The mean image was then reoriented into a standard $160 \times 160 \times 96$ voxel image grid with 1.5 mm cubic voxels. The isotropic image grid's anterior–posterior axis was oriented parallel to the subject's anterior–posterior commissure line. Each image set was then filtered with a scanner-specific filter kernel to produce images of a uniform isotropic resolution of 8 mm full-width at half-maximum, the approximate resolution of the lowest resolution scanners used in ADNI. Finally, uniform resolution ^{11}C -PiB PET images were normalized to the mean ^{11}C -PiB retention value of the cerebellar cortex providing the PiB-standardized uptake value ratio images. More detailed information can be found at http://www.loni.ucla.edu/ADNI/Data/ADNI_Data.shtml.

Each baseline PiB-standardized uptake value ratio image was co-registered to the structural MRI scan acquired at the time of the baseline ^{11}C -PiB PET scanning. A rigid body transformation algorithm (i.e. 6 degrees of freedom) based on Automated Image Registration (AIR version 5.2.6) (Woods *et al.*, 1993) was employed. Each baseline PiB-standardized uptake value ratio image was then up-sampled to the native imaging space of the corresponding structural MRI based on the estimated rigid body transformation.

Table 1 Study group demographics

<i>n</i>	61
Age at ^{11}C -PiB PET imaging baseline, years	75.5 (8.0)
Follow-up, years	1.0 (0.1)
Gender, % female	34
Education, years	16.4 (2.7)
MMSE at ^{11}C -PiB PET imaging baseline	27.0 (2.4)
GD Scale at ^{11}C -PiB PET imaging baseline	1.8 (2.1)
CDR at ^{11}C -PiB PET imaging baseline	0.5 (0.2)
ADAS-Cog at ^{11}C -PiB PET imaging baseline	11.2 (5.6)
Percent of APOE $\epsilon 4$ carriers	61

Statistics are provided in mean (standard deviation) format.

ADAS-Cog = Alzheimer Disease Assessment Scale-Cognitive; CDR = Clinical Dementia Rating; GD Scale = Geriatric Depression Scale; MMSE = Mini-Mental State Exam.

Magnetic resonance imaging acquisition

The participants at each site underwent the following standardized 1.5 T MRI protocol (<http://www.loni.ucla.edu/ADNI/Research/Cores/index.shtml>): two T_1 -weighted MRI scans, using a sagittal volumetric magnetization prepared rapid gradient echo (MP-RAGE) sequence, with an echo time of 4 ms, repetition time of 9 ms, flip angle of 8° and acquisition matrix size of $256 \times 256 \times 166$ in the x -, y - and z -dimensions with a nominal voxel size of $0.94 \times 0.94 \times 1.2$ mm. A designated centre selected the MP-RAGE image with higher quality and corrected for system-specific image artefacts such as geometry distortion, B1 non-uniformity and intensity inhomogeneities (Jack *et al.*, 2008a). A k -space post-processing technique called 'auto-correction' was implemented to correct 3D image fields that have been corrupted by bulk head motion (McGee *et al.*, 1997). The technique operates by iteratively adding phase offsets to select lines in k -space and then automatically evaluating a quantitative metric in image space such as entropy or gradient entropy. The presence, absence and severity of common artefacts (e.g. blurring due to head motion) are also indicated in the MRI quality control files. MRI scan at the time of the baseline ^{11}C -PiB PET scanning was considered as the baseline structural scan in this study and the follow-up structural scan within 1 year of this baseline structural scan was used to quantify the annual brain tissue loss rate as described below.

Unbiased magnetic resonance imaging structural brain image template

To avoid bias towards a particular subject's geometry in generating a reference brain image, we used the baseline MRI data from all subjects in this study to create an unbiased large deformation structural brain image template (Joshi *et al.*, 2004). First, the skull, scalp, extra-cranial tissue, cerebellum and brain stem (at the level of the diencephalon) were removed from each T_1 -weighted image data using the automated Brain Surface Extraction software (Shattuck and Leahy, 2002), followed by quality check. The automatically generated Brain Surface Extraction brain masks were manually refined if necessary. A study-specific unbiased large deformation template was then created using baseline structural brain images from all 61 participants with mild cognitive impairment by applying a fluid registration algorithm as described in full elsewhere (Joshi *et al.*, 2004; Lorenzen *et al.*, 2005). Briefly, unbiased large deformation template formation incorporates an unbiased approach where all baseline brain images are first simultaneously affine (i.e. 12 degrees-of-freedom) transformed to adjust for global variations in brain positioning and scale. Affine transformed subject brain images are then simultaneously deformed iteratively to yield an average unbiased large deformation template. A non-linear inverse-consistent fluid-flow deformation field from each affine transformed subject brain image to the resulting unbiased large deformation template is estimated through this process.

Creation of maps of brain atrophy rates

To compute the rate of regional brain volume change (i.e. brain atrophy rate), the 1-year follow-up T_1 -weighted MRI scan of each subject was first brain tissue masked using Brain Surface Extraction and then the data were rigid body transformed into the image space of the corresponding baseline scan. An inverse-consistent diffeomorphic fluid-flow warping algorithm was further applied to spatially normalize the registered 1-year follow-up image to the baseline brain image.

Finally, rates of regional brain volume change were computed for each subject based on the determinant of the Jacobians describing the diffeomorphic deformation fields (i.e. Jac-map), yielding maps of rates of fractional volume contraction or expansion at each voxel in each subject's native baseline image space.

^{11}C -labelled Pittsburgh compound B positron emission tomography and magnetic resonance imaging data fusion

For the joint analysis of maps of PiB-standardized uptake value ratio and brain atrophy rates, the baseline PiB-standardized uptake value ratio map (co-registered to the corresponding baseline structural magnetic resonance image) and the corresponding Jac-map of each subject were transformed to the unbiased large deformation template space using the same affine and unbiased large-deformation fluid-flow field estimated in creation of the unbiased large deformation brain template as described above and as illustrated in Fig. 1. In addition, the PiB-standardized uptake value ratio map and Jac-map were each smoothed with a Gaussian spatial kernel of 4 and 6 mm full-width at half-maximum, respectively. The 2:3 ratio of the different smoothing kernels for PiB-standardized uptake value ratio map and Jac-map was estimated according to methods described in Hagler *et al.* (2006) to achieve comparable degrees of smoothing for the two image modalities.

Joint statistical analysis of ^{11}C -labelled Pittsburgh compound B positron emission tomography and magnetic resonance imaging

In this study, we aimed to test distributed relationships between amyloid- β accumulation and 1-year brain atrophy rates across brain regions. To achieve this goal, we analysed both image modalities jointly and furthermore took all image voxels into account simultaneously using the concept of parallel independent component analysis. This analytical strategy is designed to test the hypothesis that a systematic pattern of regional amyloid- β accumulation, as reflected by PiB-standardized uptake value ratio maps, is associated with a regional pattern of 1-year brain atrophy rates, as measured with MRI Jac-maps. Importantly, this analysis makes no restrictions on local relationships between PiB-standardized uptake value ratio and Jac-map but also includes relationships that might be spatially dissociated, involving influence of amyloid- β accumulation on brain atrophy rates in distant brain regions.

The mathematical foundations of parallel independent component analysis are described in detail in Liu *et al.* (2009). We used the parallel independent component analysis package FIT (Fusion ICA Toolbox <http://icatb.sourceforge.net>) to obtain statistical maps of joint relationships. In short, parallel independent component analysis applied to multimodality imaging data aims to identify independent components in each image modality as well as the relationships of these independent components across image modalities.

In the context of this study, the parallel independent component analysis design identified spatially independent components in each PiB-standardized uptake value ratio and Jac-map of the MRI while simultaneously revealing the largest variations across the subjects with mild cognitive impairment that PiB-standardized uptake value ratio and MRI Jac-map had in common. The number of significant

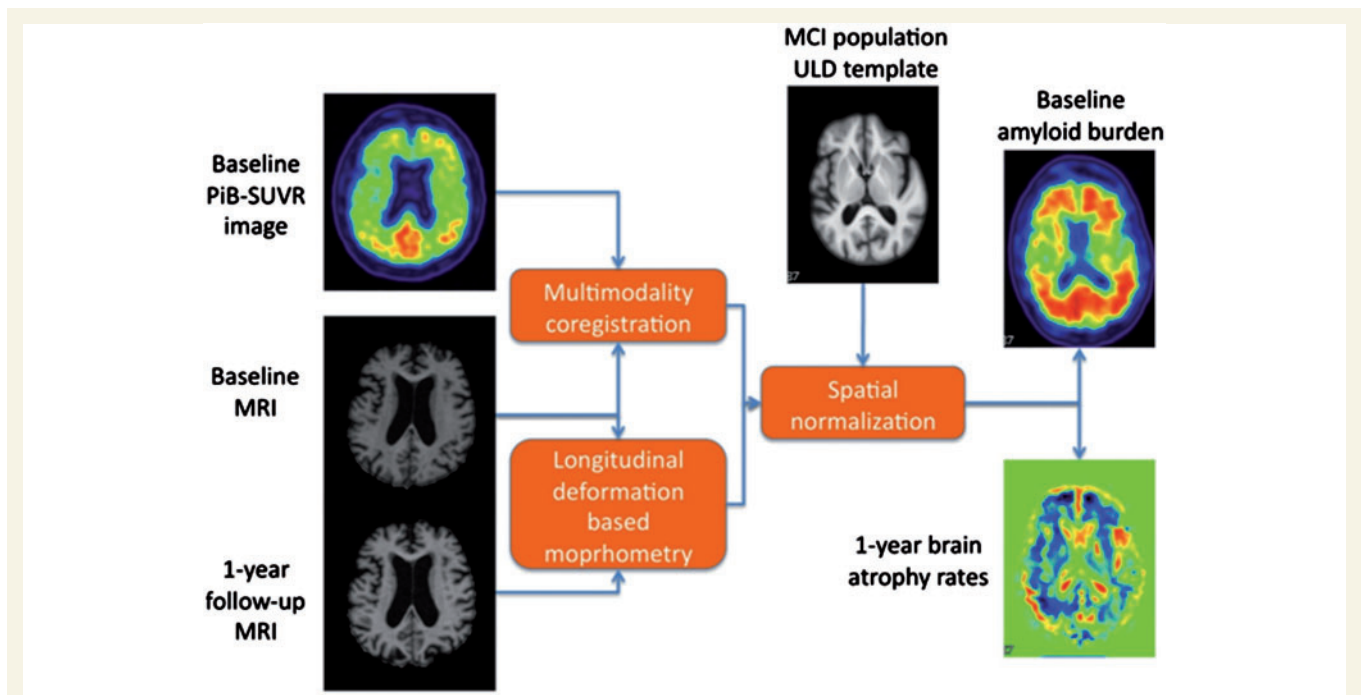


Figure 1 Data mapping of baseline PiB-standardized uptake value ratio (PiB-SUVR) and 1-year brain atrophy rates (Jac-map) for spatial statistical analysis in the unbiased large deformation (ULD) template image space. MCI = mild cognitive impairment.

independent components in each modality was estimated using both the Akaike information criterion and the minimum description length criterion (Calhoun *et al.*, 2001). For each modality, the loading parameters expressing the contribution of each independent component to the variance across subjects were estimated. Each independent component for each modality was scaled to unit standard deviation, yielding z-score maps in the unbiased large deformation template brain image space. All component maps were thresholded at a z-score level of $|z| \geq 2.5$ (99.4% cumulative probability) for visualization purposes.

Based on these loading parameters, we computed Pearson's correlation coefficients for all pairs of PiB-standardized uptake value ratio and brain atrophy rates independent components while further accounting for variations in age, gender, education levels, APOE $\epsilon 4$ carrier status, and Alzheimer Disease Assessment Scale-Cognitive test scores across the subjects with mild cognitive impairment. Alzheimer Disease Assessment Scale-Cognitive test scores were included in the model to adjust for different levels of cognitive impairment within the mild cognitive impairment group, which might skew the regional patterns of amyloid- β accumulation and brain atrophy rates as well as the relationships between them. The Pearson's correlation coefficients were then used to identify significant relationships between regional brain amyloid- β accumulation and brain atrophy rates after correction for multiple comparison using a false discovery rate at significance level of $q < 0.05$ (Benjamini and Hochberg, 1995).

Results

We found two significant and spatially distributed component pairs in mild cognitive impairment, each depicting an association between PiB-standardized uptake value ratio measures at baseline and regional brain atrophy rates over 1 year follow-up.

The spatial extent of the first significant component pair is shown in Fig. 2, overlaid onto the unbiased large deformation brain template. The first component pair showed a partial correlation of 0.77 between baseline PiB-standardized uptake value ratio and regional brain atrophy rates with a false discovery rate corrected significance level of $P = 0.0004$. The adjusted R^2 value of the fitted model for this component pair was 0.58 with $P < 10^{-4}$. The brain regions identified by this first component pair, as shown in Table 2, imply more amyloid- β burden was associated with higher rates of brain atrophy. Regions with increased amyloid- β burden included the precuneus, cuneus, medial temporal (including fusiform, lingual, entorhinal), inferior parietal regions in the left hemisphere, bilateral posterior cingulate and right lateral fronto-orbital regions. Interestingly, a predominantly left-sided increase in amyloid- β burden in these brain regions was associated with higher atrophy rates (i.e. more grey matter and white matter tissue loss and larger sulcal cerebro-spinal fluid expansion over a 1-year period) in the medial temporal regions (including entorhinal, fusiform, parahippocampal), amygdala, inferior temporal, superior frontal, inferior frontal in the left hemisphere, bilateral posterior cingulate and left cerebellum.

We further found a second significant component pair. The spatial extent of the second significant component pair is shown in Fig. 3, overlaid onto the unbiased large deformation brain template. The adjusted R^2 value of the fitted model for the second component pair was 0.34 ($P < 0.0001$) and the partial correlation coefficient between the baseline PiB-standardized uptake value ratio and regional brain atrophy rates was 0.65 (false discovery rate corrected $P = 0.04$). In the second component pair, increased amyloid- β burden in bilateral precuneus/cuneus, bilateral posterior

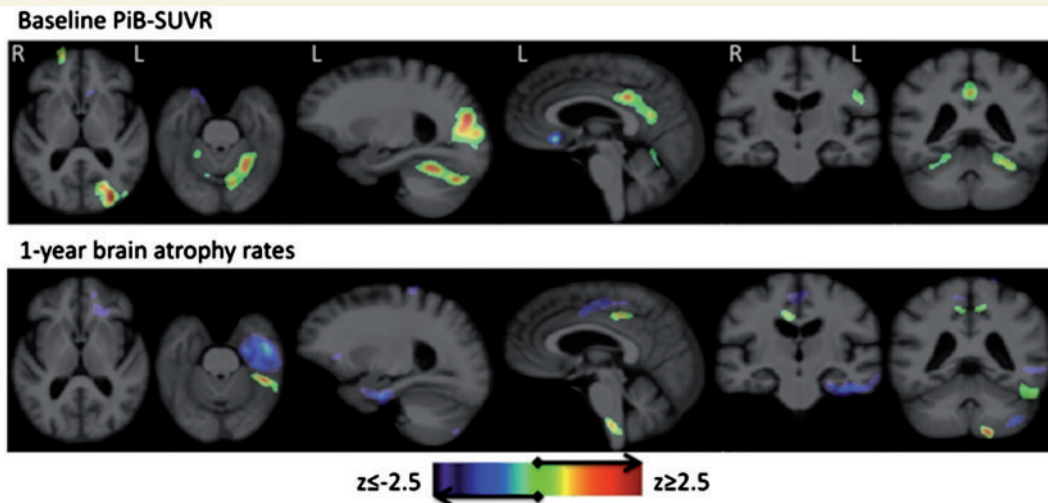


Figure 2 First parallel independent component analysis component pair. SUVR = standardized uptake value ratio.

Table 2 Regions of the associated baseline amyloid- β and 1-year brain atrophy rates components identified by parallel independent component analysis

Baseline PiB-standardized uptake value ratio		1-year brain atrophy rates (in mm^3)	
Region	Mean \pm SD	Region	Mean \pm SD (%)
First parallel independent component analysis component pair			
Left precuneus/cuneus	1.66 \pm 0.52	Left amygdala	-0.24 \pm 5.05
Left inferior parietal	2.06 \pm 0.62	Left inferior temporal	-2.56 \pm 6.42
Bilateral posterior cingulate	2.22 \pm 0.70	Left superior frontal	-1.14 \pm 8.21
Right lateral fronto-orbital	2.25 \pm 0.82	Left cerebellum	-3.90 \pm 8.53
Left medial temporal (fusiform, lingual, entorhinal)	2.07 \pm 0.58	Bilateral posterior cingulate	-0.71 \pm 2.71
		Left medial temporal regions (entorhinal, fusiform, parahippocampal)	-2.75 \pm 2.81
Second parallel independent component analysis component pair			
Bilateral precuneus/cuneus	2.08 \pm 0.79	Left parahippocampus	2.83 \pm 8.65
Bilateral posterior cingulate	1.78 \pm 0.62	Right amygdala	-0.87 \pm 3.80
Left inferior frontal	1.76 \pm 0.64	Right middle fronto-orbital and gyrus rectus	-6.83 \pm 7.36
Left inferior parietal	2.09 \pm 0.55	Right medial temporal regions (entorhinal, fusiform, parahippocampal, subcallosal)	-0.52 \pm 6.07
Left superior parietal	1.44 \pm 0.59		
Bilateral thalamus regions	1.86 \pm 0.22		

cingulate, left inferior frontal, left inferior parietal, left superior parietal and bilateral thalamus regions was associated with higher atrophy rates in the right medial temporal regions (including entorhinal, fusiform, parahippocampal, subcallosal), right amygdala, right middle fronto-orbital, right gyrus rectus and left parahippocampus, as shown in Table 2. Note, each of the two significant component pairs from the parallel independent component analysis identifies a spatially distributed pattern of regions with high amyloid- β burden and regions with high rates of brain atrophy in mild cognitive impairment, as seen in the voxel-wise overlay in Figs 2 and 3.

We also explored the possibility that the relationship between PiB-standardized uptake value ratio measures and brain atrophy rates were not simply an artefact of partial-volume effects of PiB data. We tested this by computing a grey matter index from tissue segmented MRI data obtained at baseline for each region of interest where a significant relationship between PiB-standardized uptake value ratio and brain atrophy rates were found and then repeating the analysis with the grey matter index as an additional covariate to account for partial-volume effects of PiB data. We found that the inclusion of a grey matter index reduced relations by $\sim 1\%$ (where significance of variability due to partial-volume

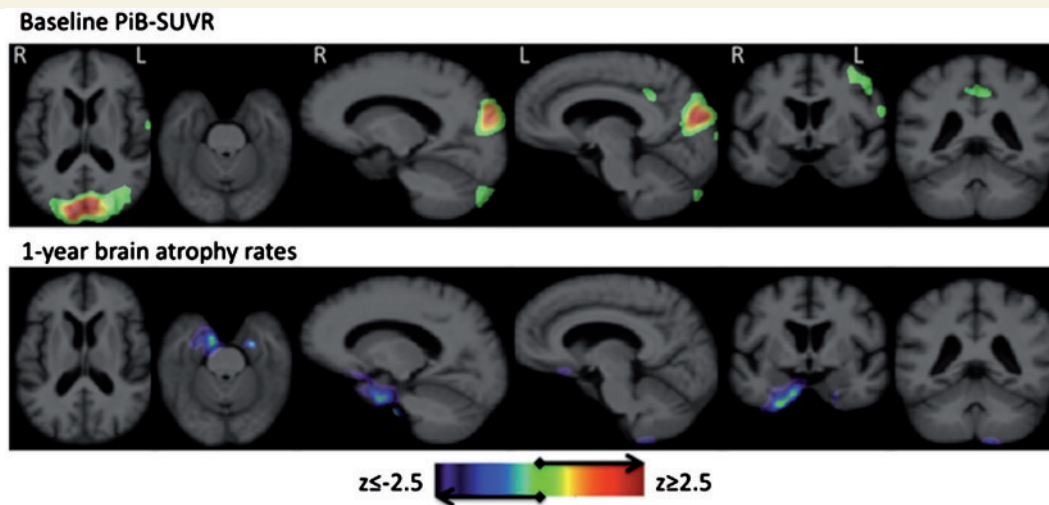


Figure 3 Second parallel independent component analysis component pair. SUVR = standardized uptake value ratio.

effect was $P = 0.60$) for the first component of parallel independent components analysis and by 7% (where significance of variability due to partial-volume effect was $P = 0.17$) for the second component, suggesting that the relationships between amyloid- β load and brain atrophy rates cannot simply be explained as partial-volume artefacts.

Discussion

There are two major findings in this study: first, high amyloid- β levels, detected by ^{11}C -PiB PET imaging, in mild cognitive impairment are associated with increased brain atrophy rates, detected by longitudinal MRI. The finding adds to the generally held view that patients with mild cognitive impairment who have amyloid- β pathology have high brain atrophy rates and are likely to progress to Alzheimer's disease within a relatively short time, while subjects with mild cognitive impairment without amyloid- β pathology have much lower brain atrophy rates and may not develop Alzheimer's disease. Second, the spatial distribution of increased amyloid- β and the associated spatial distribution of increased brain atrophy rates embrace a characteristic pattern of brain structures known for a high vulnerability to Alzheimer's disease pathology.

The finding of an association between increased amyloid- β and increased brain atrophy rates in mild cognitive impairment implies that aggregated amyloid- β leads to a progressive loss of brain tissue over time as opposed to a static loss from random insults. Although a progressive tissue loss due to increased amyloid- β deposition is expected (Jack *et al.*, 2009), an interesting observation of our study is that the regional distribution of increased amyloid- β and that of increased rates of brain tissue loss are not necessarily overlapping in mild cognitive impairment. Specifically, the joint analysis of ^{11}C -PiB PET and structural MRI data identified two component pairs of spatially distributed relations between amyloid- β deposition and brain atrophy rates. In the first component pair, high amyloid- β burden in the left precuneus/cuneus and

posterior cingulate regions was associated with increased rates of brain tissue loss primarily in the left medial temporal lobe, including the entorhinal cortex and parahippocampal gyrus. On the other hand, in the second component pair, high amyloid- β burden in bilateral precuneus/cuneus and posterior cingulate region was associated with increased rates of brain tissue loss primarily in the right medial temporal lobe regions. Taken together, these results may begin to shed light on the mechanisms by which regionally selective amyloid- β deposition in mild cognitive impairment leads to a spatial pattern of distributed neurodegeneration, which resembles that seen in Alzheimer's disease. Potentially, these mechanisms are anterograde and selectively target the memory networks. The systematic patterns of increased amyloid- β burden and increased brain atrophy rates in the patients with mild cognitive impairment, strongly resembling the pattern typically seen in Alzheimer's disease, further supports the view that these relations reflect brain alterations presymptomatic to Alzheimer's disease and could be useful for staging disease severity and for monitoring treatment interventions in preclinical stages of Alzheimer's disease.

Structural MRI studies in Alzheimer's disease have consistently revealed a pattern of neuroanatomical abnormalities that predominantly involve structures in the medial temporal cortex (i.e. hippocampus and the entorhinal cortex) (Du *et al.*, 2001, 2003, 2004; deToledo-Morrell *et al.*, 2004; Thompson *et al.*, 2004; Hampel *et al.*, 2005; Stoub *et al.*, 2005; Morra *et al.*, 2008, 2009a, b; Schroeter *et al.*, 2009) where the early pathological changes are seen, then gradually extends to temporoparietal cortical areas (Chetelat and Baron, 2003; Whitwell *et al.*, 2007, 2008; Desikan *et al.*, 2008; Hua *et al.*, 2008) as severity of Alzheimer's disease progresses (Jack *et al.*, 2004, 2005, 2008c; DeCarli *et al.*, 2007; Whitwell *et al.*, 2007, 2008). Findings in both parallel independent component analysis component pairs point to a selective vulnerability of these regions to Alzheimer's disease pathology, consistent with histopathological findings. The finding in mild cognitive impairment that a localized distribution of amyloid- β deposition is

associated with a characteristic pattern of brain atrophy that resembles the atrophy pattern seen in Alzheimer's disease is encouraging for the use of ^{11}C -PiB-PET measures as early indicators of Alzheimer's disease. Most importantly, elucidating the detrimental relationship between the local amyloid- β burden and rates of brain atrophy is of great interest to enhance our understanding of the underlying mechanisms of disease and use of this knowledge in development of new anti-therapies for Alzheimer's disease.

Another important observation is the prominence of the left hemisphere in the relationship between increased amyloid- β burden and increased rates of brain atrophy. This observation is consistent with previous reports of higher atrophy rates on the left hemisphere compared with the right hemisphere in patients with Alzheimer's disease (Thompson *et al.*, 2003). It is also interesting in comparison to other MRI studies, which found a trend of higher right than left asymmetry of hippocampal atrophy rates in cognitively normal elderly subjects and some evidence that suggests there is a change in asymmetry during the progression toward Alzheimer's disease (Barnes *et al.*, 2005). It is therefore possible that the laterality in brain atrophy rates that we observed in the first parallel independent component analysis component pair is another potentially useful index for staging Alzheimer's disease severity as well as for assessing disease-altering interventions. Further prospective studies of joint ^{11}C -PiB PET and MRI evaluations including elderly individuals without cognitive deficits are warranted to determine the value of asymmetric findings for an early detection of Alzheimer's disease pathology.

Another interesting observation in this study is a marked dissimilarity between the spatial distributions of increased amyloid- β deposition and that of increased brain atrophy rates in mild cognitive impairment. In particular, the spatial dissimilarity between increased amyloid- β deposition that included the precuneus and cingulate cortex whereas increased atrophy rates involved mainly medial temporal lobe structures but left precuneus and the cingulate cortex largely unaffected, is unexpected. It is possible that the brain regions with increased amyloid- β deposition in patients with mild cognitive impairment has already reached an equilibrium or plateau in terms of the rate of atrophy very early in the course of Alzheimer's disease while atrophy rates in regions with low amyloid- β burden are further progressing. This interpretation is also consistent with the paradigm that amyloid- β is the first indication of disease and higher atrophy rates are a downstream process. From a functional anatomy point of view, the precuneus is implicated in the recollection of past episodes whereas posterior cingulate projecting from thalamus and neocortex to entorhinal cortex via cingulum fibres is characteristically active during recall and deactivated during encoding of episodic memory (Cabeza and Nyberg, 2000). Cognitive decline in episodic memory is one of the earliest clinical syndromes of Alzheimer's disease. A popular hypothesis on disease mechanism suggests that amyloid- β accumulation is responsible for brain atrophy and hence the cognitive decline (Jack *et al.*, 2010). According to this hypothesis, our findings together with the functional role of precuneus and posterior cingulate regions suggest that anti-amyloid- β therapy might be successful when administered very early in the disease evolution before the synaptic and neuronal loss in brain regions susceptible

to early amyloid- β deposition reach a plateau. In a related investigation, Driscoll *et al.* (2010) reported no association between amyloid- β burden and rates of brain atrophy in the preceding years in healthy elderly individuals. Their finding suggests that either ageing-related structural brain atrophy rates are independent of amyloid- β deposition, or amyloid- β deposition must reach a particular level and be present for an extended time period before causing extensive Alzheimer's disease-related brain atrophy. To further elucidate these hypotheses future studies focusing on especially early mild cognitive impairment populations are needed. In addition, the use of a selective *in vivo* marker of regional aggregated tau deposition in the form of neurofibrillary tangles would be useful to assess the linkage between regional amyloid- β , regional neurofibrillary tangle deposition and regional atrophy rates. To date, no useful neurofibrillary tangle-specific imaging agent has been conclusively demonstrated.

An important conceptual difference between our study and other imaging studies in mild cognitive impairment is the approach to jointly evaluate not only variations across the two imaging modalities, but also variations that the imaging modalities have in common across brain regions. This approach provided insight into the spatial distributions of amyloid- β and brain atrophy rate relations that conventional analysis methods, which test relationships by regions of interest or voxel-by-voxel, cannot provide. The difference in methods may also explain the differences in findings between our studies and others. For example, other ^{11}C -PiB-PET studies found higher amyloid- β depositions also in other brain regions, including the frontal, posterior cingulate, parietal, and lateral temporal cortices, as well as in the subcortical regions including caudate and putamen (Kemppainen *et al.*, 2007; Rowe *et al.*, 2007). Similarly, other MRI studies in mild cognitive impairment have also found significant atrophy in temporal lobe white matter, orbitofrontal and medial prefrontal grey matter, posterior cingulate, insula and uncus (Apostolova *et al.*, 2006; Becker *et al.*, 2006; Colliot *et al.*, 2008; Fan *et al.*, 2008). However, the variations in amyloid- β and brain atrophy rates in these regions might be independent of each other, which would explain our inability to detect significant variations in these regions with parallel independent component analysis. Although another study reported no significant relationship between increased amyloid- β and brain atrophy in mild cognitive impairment, the authors suggested a concordance between atrophy and amyloid- β deposition in the posterior cingulate, precuneus and lateral temporoparietal association cortices during early stages of the disease process (Chetelat *et al.*, 2010). Lack of an amyloid- β -brain atrophy rate association, especially in posterior cingulate and precuneus regions, is a surprising finding of our study. An explanation would be that reduced ^{11}C -PiB signal due to atrophy in these regions would affect our ability to detect a local relationship between amyloid- β deposition and atrophy progression, since we chose to analyse non-atrophy-corrected PiB-standardized uptake value ratio data.

Amyloid- β levels in CSF have also been proposed as a diagnostic biomarker for Alzheimer's disease by various researchers (Andreasen *et al.*, 1999; Blennow and Hampel, 2003; Clark *et al.*, 2003; Bouwman *et al.*, 2007; De Meyer *et al.*, 2010; Fjell *et al.*, 2010). Recently, we reported that lower CSF amyloid- β_{1-42} concentrations were associated with higher rates of brain volume

loss in the left temporal and parietal cortices (Tosun *et al.*, 2010) in mild cognitive impairment, similar to our findings of higher amyloid- β levels in the brain from this study. Furthermore, significant correlation ($r = -0.72$) between the global ^{11}C -PiB binding load and the CSF amyloid- β_{1-42} concentrations were found across healthy elderly, mild cognitive impairment and Alzheimer's disease populations (Jagust *et al.*, 2009; Tolboom *et al.*, 2009a). Taken together, these findings also encourage the use of ^{11}C -PiB-PET imaging measures as early indicators of Alzheimer's disease.

In Alzheimer's disease, the default-mode network is markedly disconnected compared with healthy elderly controls, especially in the bilateral calcarine/cuneus, bilateral precuneus/post-cingulate, left lingual, left middle temporal gyrus, left parahippocampal, right angular, right dorsolateral prefrontal cortices as well as in the left hippocampus (Greicius *et al.*, 2004; Zhou *et al.*, 2010). It has been hypothesized that disruption of functional connectivity within default-mode network could be an alternative biomarker to structural alterations for early diagnosis of Alzheimer's disease (Hedden *et al.*, 2009; Yvette *et al.*, 2010). Moreover, it has been suggested that destabilization of neuronal networks and compensatory responses contribute to cognitive impairments in Alzheimer's disease and that such destabilization stems, at least in part, from aberrant increases in neuronal activity induced by high amyloid- β levels (Palop and Mucke, 2009). Regions with high amyloid- β deposition and associated accelerated atrophy also mirror the regions affected in default-mode network. In particular, posterior components of the default-mode network, including the precuneus and posterior cingulate, are particularly vulnerable to early deposition of amyloid- β (Braak and Braak, 1991) and the temporal components of the default-mode network are mentioned in regional atrophy early in the disease process. One interpretation of these observations is that amyloid- β pathology could be linked to neural dysfunction in a distributed network of brain regions linked to memory function (Sperling *et al.*, 2009). An important question is if default-mode network dysfunction is a functional consequence of amyloid- β deposition, especially since increased neuronal activity has been shown to increase the production, release and/or accumulation of amyloid- β , raising the possibility of a vicious cycle in which amyloid- β promotes its own production through alterations in neuronal network activity (Kamenetz *et al.*, 2003; Cirrito *et al.*, 2005). Further longitudinal studies are required to better understand such a causality between amyloid- β deposition and default-mode network dysfunction.

Several limitations of our study ought to be mentioned. First, mild cognitive impairment subjects are notoriously a very heterogeneous group and other pathologies, unrelated to Alzheimer's disease, may have contributed to variations in both amyloid- β and rates of brain atrophy. In addition, we did not separate patients with mild cognitive impairment with high PiB burden and high atrophy rates from those with low PiB burden and low atrophy rates to maintain sufficient statistical power. By analysing the groups together, we may have underestimated the extent of joint variations in amyloid- β and atrophy rate in the high PiB burden/atrophy rate group of mild cognitive impairment and similarly, overestimated these variations in the low PiB burden/atrophy rate group. The value of our findings to predict Alzheimer's

disease remains uncertain because the number of patients with mild cognitive impairment who had ^{11}C -PiB PET and converted to Alzheimer's disease was small at the time of this study. In addition, the number of cognitively normal subjects in ADNI, who had both ^{11}C -PiB PET and sequential MRI scans at the time of the study was too small for a reliable statistical analysis. Therefore, the extent to which our findings separate mild cognitive impairment from cognitively normal subjects or have value to predict who will develop mild cognitive impairment is unclear.

Our study also has several technical limitations. First, errors in image registrations between the image modalities as well as errors in spatial normalization may have increased variability and hence diminished statistical power to detect intrinsic relationships between atrophy rates and amyloid- β burden at a localized level. Second, the current framework of parallel independent component analysis assumes that measurements in each image voxel are independent and noise is identically distributed, which is likely not true and therefore statistical evaluations could be inflated.

In conclusion, our major finding links a greater amyloid- β deposition in the precuneus, a region generally known for early accumulation of amyloid plaques, to a unique pattern of increased brain atrophy within each hemisphere, resembling the pattern seen also in Alzheimer's disease. These results may begin to shed light on the mechanisms by which amyloid- β deposition leads to neurodegeneration and cognitive decline and the development of a more specific Alzheimer's disease-specific imaging signature for diagnosis.

Funding

This work is funded by the National Institutes of Health (NIH) (Grant P41 RR023953). Data collection and sharing for this project were funded by the Alzheimer's Disease Neuroimaging Initiative (ADNI) (NIH Grant U01 AG024904). ADNI is funded by the National Institute on Aging, the National Institute of Biomedical Imaging and Bioengineering, and through generous contributions from the following: Abbott, AstraZeneca AB, Bayer Schering Pharma AG, Bristol-Myers Squibb, Eisai Global Clinical Development, Elan Corporation, Genentech, GE Healthcare, GlaxoSmithKline, Innogenetics, Johnson and Johnson, Eli Lilly and Co., Medpace, Inc., Merck and Co., Inc., Novartis AG, Pfizer Inc, F. Hoffman-La Roche, Schering-Plough, Synarc, Inc. and Wyeth, as well as non-profit partners the Alzheimer's Association and Alzheimer's Drug Discovery Foundation, with participation from the US Food and Drug Administration. Private sector contributions to ADNI are facilitated by the Foundation for the National Institutes of Health (www.fnih.org). The grantee organization is the Northern California Institute for Research and Education, and the study is coordinated by the Alzheimer's Disease Cooperative Study at the University of California, San Diego, USA. ADNI data are disseminated by the Laboratory for Neuro Imaging at the University of California, Los Angeles. This research was also supported by NIH grants (P30 AG010129, K01 AG030514) and the Dana Foundation.

References

- Aizenstein HJ, Nebes RD, Saxton JA, Price JC, Mathis CA, Tsopelas ND, et al. Frequent amyloid deposition without significant cognitive impairment among the elderly. *Arch Neurol* 2008; 65: 1509–17.
- Andreasen N, Minthon L, Vanmechelen E, Vanderstichele H, Davidsson P, Winblad B, et al. Cerebrospinal fluid tau and A[β]42 as predictors of development of Alzheimer's disease in patients with mild cognitive impairment. *Neurosci Lett* 1999; 273: 5–8.
- Apostolova LG, Dinov ID, Dutton RA, Hayashi KM, Toga AW, Cummings JL, et al. 3D comparison of hippocampal atrophy in amnesic mild cognitive impairment and Alzheimer's disease. *Brain* 2006; 129: 2867–73.
- Archer HA, Edison P, Brooks DJ, Barnes J, Frost C, Yeatman T, et al. Amyloid load and cerebral atrophy in Alzheimer's disease: an 11C-PIB positron emission tomography study. *Ann Neurol* 2006; 60: 145–7.
- Barnes J, Scahill RI, Schott JM, Frost C, Rossor MN, Fox NC. Does Alzheimer's disease affect hippocampal asymmetry? evidence from a cross-sectional and longitudinal volumetric MRI study. *Dement Geriatr Cogn Disord* 2005; 19: 338–44.
- Becker JT, Davis SW, Hayashi KM, Meltzer CC, Toga AW, Lopez OL, et al. Three-dimensional patterns of hippocampal atrophy in mild cognitive impairment. *Arch Neurol* 2006; 63: 97–101.
- Benjamini Y, Hochberg Y. Controlling the false discovery rate: a practical and powerful approach to multiple testing. *J R Statist Soc B Methodol* 1995; 57: 289–300.
- Blennow K, Hampel H. CSF markers for incipient Alzheimer's disease. *Lancet Neurol* 2003; 2: 605–13.
- Bourgeat P, Chételat G, Villemagne VL, Fripp J, Raniga P, Pike K, et al. β -Amyloid burden in the temporal neocortex is related to hippocampal atrophy in elderly subjects without dementia. *Neurology* 2010; 74: 121–7.
- Bouwman FH, Schoonenboom SNM, van der Flier WM, van Elk EJ, Kok A, Barkhof F, et al. CSF biomarkers and medial temporal lobe atrophy predict dementia in mild cognitive impairment. *Neurobiol Aging* 2007; 28: 1070–4.
- Braak H, Braak E. Neuropathological staging of Alzheimer-related changes. *Acta Neuropathol* 1991; 82: 239–59.
- Cabeza R, Nyberg L. Imaging cognition II: an empirical review of 275 PET and fMRI studies. *J Cogn Neurosci* 2000; 12: 1–47.
- Calhoun VD, Adali T. Feature-based fusion of medical imaging data. *IEEE Trans Inf Technol Biomed* 2009; 13: 711–20.
- Calhoun VD, Adali T, Pearlson GD, Pekar JJ. A method for making group inferences from functional MRI data using independent component analysis. *Hum Brain Mapp* 2001; 14: 140–51.
- Chételat G, Baron J-C. Early diagnosis of Alzheimer's disease: contribution of structural neuroimaging. *NeuroImage* 2003; 18: 525–41.
- Chételat G, Villemagne VL, Bourgeat P, Pike KE, Jones G, Ames D, et al. Relationship between atrophy and beta-amyloid deposition in Alzheimer disease. *Ann Neurol* 2010; 67: 317–24.
- Cirrito JR, Yamada KA, Finn MB, Sloviter RS, Bales KR, May PC, et al. Synaptic activity regulates interstitial fluid amyloid- \leq levels in vivo. *Neuron* 2005; 48: 913–22.
- Clark CM, Xie S, Chittams J, Ewbank D, Peskind E, Galasko D, et al. Cerebrospinal fluid tau and β -amyloid: how well do these biomarkers reflect autopsy-confirmed dementia diagnoses? *Arch Neurol* 2003; 60: 1696–702.
- Colliot O, Chételat G, Chupin M, Desgranges B, Magnin B, Benali H, et al. Discrimination between Alzheimer disease, mild cognitive impairment, and normal aging by using automated segmentation of the hippocampus. *Radiology* 2008; 248: 194–201.
- DeCarli C, Frisoni GB, Clark CM, Harvey D, Grundman M, Petersen RC, et al. Qualitative estimates of medial temporal atrophy as a predictor of progression from mild cognitive impairment to dementia. *Arch Neurol* 2007; 64: 108–15.
- De Meyer G, Shapiro F, Vanderstichele H, Vanmechelen E, Engelborghs S, De Deyn PP, et al. Diagnosis-independent Alzheimer disease biomarker signature in cognitively normal elderly people. *Arch Neurol* 2010; 67: 949–56.
- Desikan RS, Fischl B, Cabral HJ, Kemper TL, Guttman CRG, Blacker D, et al. MRI measures of temporoparietal regions show differential rates of atrophy during prodromal Alzheimer's disease. *Neurology* 2008; 71: 819–25.
- deToledo-Morrell L, Stoub TR, Bulgakova M, Wilson RS, Bennett DA, Leurgans S, et al. MRI-derived entorhinal volume is a good predictor of conversion from mild cognitive impairment to Alzheimer's disease. *Neurobiol Aging* 2004; 25: 1197–203.
- Devanand DP, Mikhno A, Pelton GH, Cuasay K, Pradhaban G, Dileep Kumar JS, et al. Pittsburgh compound B (11C-PIB) and fluorodeoxyglucose (18 F-FDG) PET in patients with Alzheimer disease, mild cognitive impairment, and healthy controls. *J Geriatr Psychiatry Neurol* 2010; 23: 185–98.
- Driscoll I, Resnick SM, Troncoso JC, An Y, O'Brien R, Zonderman AB. Impact of Alzheimer's pathology on cognitive trajectories in nondemented elderly. *Ann Neurol* 2006; 60: 688–95.
- Driscoll I, Zhou Y, An Y, Sojkova J, Davatzikos C, Kraut MA, et al. Lack of association between 11C-PIB and longitudinal brain atrophy in non-demented older individuals. *Neurobiol Aging* 2010; doi:10.1016/j.neurobiolaging.2009.12.008.
- Du AT, Schuff N, Amend D, Laakso MP, Hsu YY, Jagust WJ, et al. Magnetic resonance imaging of the entorhinal cortex and hippocampus in mild cognitive impairment and Alzheimer's disease. *J Neurol Neurosurg Psychiatry* 2001; 71: 441–7.
- Du AT, Schuff N, Kramer JH, Ganzer S, Zhu XP, Jagust WJ, et al. Higher atrophy rate of entorhinal cortex than hippocampus in Alzheimer's disease. *Neurology* 2004; 62: 422–7.
- Du AT, Schuff N, Zhu XP, Jagust WJ, Miller BL, Reed BR, et al. Atrophy rates of entorhinal cortex in Alzheimer's disease and normal aging. *Neurology* 2003; 60: 481–6.
- Edison P, Archer HA, Hinz R, Hammers A, Pavese N, Tai YF, et al. Amyloid, hypometabolism, and cognition in Alzheimer disease: an [11C]PIB and [18F]FDG PET study. *Neurology* 2007; 68: 501–8.
- Fan Y, Batmanghelich N, Clark CM, Davatzikos C. Spatial patterns of brain atrophy in mild cognitive impairment patients, identified via high-dimensional pattern classification, predict subsequent cognitive decline. *NeuroImage* 2008; 39: 1731–43.
- Fjell AM, Walhovd KB, Fennema-Notestine C, McEvoy LK, Hagler DJ, Holland D, et al. CSF Biomarkers in Prediction of Cerebral and Clinical Change in Mild Cognitive Impairment and Alzheimer's Disease. *J Neurosci* 2010; 30: 2088–101.
- Folstein MF, Folstein SE, McHugh PR. 'Mini-mental state': a practical method for grading the cognitive state of patients for the clinician. *J Psychiatr Res* 1975; 12: 189–98.
- Fotinos AF, Mintun MA, Snyder AZ, Morris JC, Buckner RL. Brain volume decline in aging: evidence for a relation between socioeconomic status, preclinical Alzheimer disease, and reserve. *Arch Neurol* 2008; 65: 113–20.
- Frisoni GB, Lorenzi M, Caroli A, Kempainen N, Nagren K, Rinne JO. In vivo mapping of amyloid toxicity in Alzheimer disease. *Neurology* 2009; 72: 1504–11.
- Forsberg A, Engler H, Almkvist O, Blomquist G, Hagman G, Wall A, et al. PET imaging of amyloid deposition in patients with mild cognitive impairment. *Neurobiol Aging* 2008; 29: 1456–65.
- Galvin JE, Powlisha KK, Wilkins K, McKeel DW Jr, Xiong C, Grant E, et al. Predictors of preclinical Alzheimer disease and dementia: a clinicopathologic study. *Arch Neurol* 2005; 62: 758–65.
- Greicius MD, Srivastava G, Reiss AL, Menon V. Default-mode network activity distinguishes Alzheimer's disease from healthy aging: evidence from functional MRI. *Proc Natl Acad Sci USA* 2004; 101: 4637–42.
- Hagler DJ Jr, Saygin AP, Sereno MI. Smoothing and cluster thresholding for cortical surface-based group analysis of fMRI data. *NeuroImage* 2006; 33: 1093–103.
- Hampel H, Burger K, Pruessner JC, Zinkowski R, DeBernardis J, Kerkman D, et al. Correlation of cerebrospinal fluid levels of tau

- protein phosphorylated at threonine 231 with rates of hippocampal atrophy in Alzheimer disease. *Arch Neurol* 2005; 62: 770–3.
- Hedden T, Van Dijk KRA, Becker JA, Mehta A, Sperling RA, Johnson KA, et al. Disruption of functional connectivity in clinically normal older adults harboring amyloid burden. *J Neurosci* 2009; 29: 12686–94.
- Hua X, Leow AD, Lee S, Klunder AD, Toga AW, Lepore N, et al. 3D characterization of brain atrophy in Alzheimer's disease and mild cognitive impairment using tensor-based morphometry. *NeuroImage* 2008; 41: 19–34.
- Jack CR Jr, Shiung MM, Gunter JL, O'Brien PC, Weigand SD, Knopman DS, et al. Comparison of different MRI brain atrophy rate measures with clinical disease progression in Alzheimer's disease. *Neurology* 2004; 62: 591–600.
- Jack CR Jr, Shiung MM, Weigand SD, O'Brien PC, Gunter JL, Boeve BF, et al. Brain atrophy rates predict subsequent clinical conversion in normal elderly and amnesic mild cognitive impairment. *Neurology* 2005; 65: 1227–31.
- Jack CR Jr, Bernstein MA, Fox NC, Thompson P, Alexander G, Harvey D, et al. The Alzheimer's disease neuroimaging initiative (ADNI): MRI methods. *J Magn Reson Imaging* 2008a; 27: 685–91.
- Jack CR Jr, Lowe VJ, Senjem ML, Weigand SD, Kemp BJ, Shiung MM, et al. 11C PIB and structural MRI provide complementary information in imaging of Alzheimer's disease and amnesic mild cognitive impairment. *Brain* 2008b; 131: 665–80.
- Jack CR Jr, Weigand SD, Shiung MM, Przybelski SA, O'Brien PC, Gunter JL, et al. Atrophy rates accelerate in amnesic mild cognitive impairment. *Neurology* 2008c; 70: 1740–52.
- Jack CR Jr, Lowe VJ, Weigand SD, Wiste HJ, Senjem ML, Knopman DS, et al. Serial PIB and MRI in normal, mild cognitive impairment and Alzheimer's disease: implications for sequence of pathological events in Alzheimer's disease. *Brain* 2009; 132: 1355–65.
- Jack CR Jr, Knopman DS, Jagust WJ, Shaw LM, Aisen PS, Weiner MW, et al. Hypothetical model of dynamic biomarkers of the Alzheimer's pathological cascade. *Lancet Neurol* 2010; 9: 119–28.
- Jagust WJ, Landau SM, Shaw LM, Trojanowski JQ, Koeppe RA, Reiman EM, et al. Relationships between biomarkers in aging and dementia. *Neurology* 2009; 73: 1193–9.
- Joshi S, Davis B, Jomier M, Gerig G. Unbiased diffeomorphic atlas construction for computational anatomy. *NeuroImage* 2004; 23 (Suppl 1): S151–60.
- Kamenetz F, Tomita T, Hsieh H, Seabrook G, Borchelt D, Iwatsubo T, et al. APP processing and synaptic function. *Neuron* 2003; 37: 925–37.
- Kemppainen NM, Aalto S, Wilson IA, Nagren K, Helin S, Bruck A, et al. Voxel-based analysis of PET amyloid ligand [11C]PIB uptake in Alzheimer disease. *Neurology* 2006; 67: 1575–80.
- Kemppainen NM, Aalto S, Wilson IA, Nagren K, Helin S, Bruck A, et al. PET amyloid ligand [11C]PIB uptake is increased in mild cognitive impairment. *Neurology* 2007; 68: 1603–6.
- Klunk WE, Engler H, Nordberg A, Wang Y, Blomqvist G, Holt DP, et al. Imaging brain amyloid in Alzheimer's disease with Pittsburgh Compound-B. *Ann Neurol* 2004; 55: 306–19.
- Liu J, Pearson G, Windemuth A, Ruano G, Perrone-Bizzozero NI, Calhoun V. Combining fMRI and SNP data to investigate connections between brain function and genetics using parallel ICA. *Hum Brain Mapp* 2009; 30: 241–55.
- Lockhart A. Imaging Alzheimer's disease pathology: one target, many ligands. *Drug Discov Today* 2006; 11: 1093–9.
- Lopez OL, Kuller LH, Becker JT, Dulberg C, Sweet RA, Gach HM, et al. Incidence of dementia in mild cognitive impairment in the cardiovascular health study cognition study. *Arch Neurol* 2007; 64: 416–20.
- Lorenzen P, Davis B, Joshi S. Unbiased atlas formation via large deformations metric mapping. *Med Image Comput Comput Assist Interv* 2005; 8 (Pt 2): 411–8.
- Mathis CA, Lopresti BJ, Klunk WE. Impact of amyloid imaging on drug development in Alzheimer's disease. *Nucl Med Biol* 2007; 34: 809–22.
- McGee KP, Grimm RC, Felmlee JP, Rydberg JR, Riederer SJ, Ehman RL. The shoulder: adaptive motion correction of MR images. *Radiology* 1997; 205: 541–5.
- Mikhno A, Devanand D, Pelton G, Cuasay K, Gunn R, Upton N, et al. Voxel-based analysis of 11C-PIB scans for diagnosing Alzheimer's disease. *J Nucl Med* 2008; 49: 1262–9.
- Mintun M. Utilizing advanced imaging and surrogate markers across the spectrum of Alzheimer's disease. *CNS Spectr* 2005; 10 (11 Suppl 18): 13–6.
- Mintun MA, LaRossa GN, Sheline YI, Dence CS, Lee SY, Mach RH, et al. [11C]PIB in a nondemented population: potential antecedent marker of Alzheimer disease. *Neurology* 2006; 67: 446–52.
- Mormino EC, Kluth JT, Madison CM, Rabinovici GD, Baker SL, Miller BL, et al. Episodic memory loss is related to hippocampal-mediated β -amyloid deposition in elderly subjects. *Brain* 2009; 132: 1310–23.
- Morra JH, Tu Z, Apostolova LG, Green AE, Avedissian C, Madsen SK, et al. Validation of a fully automated 3D hippocampal segmentation method using subjects with Alzheimer's disease mild cognitive impairment, and elderly controls. *NeuroImage* 2008; 43: 59–68.
- Morra JH, Tu Z, Apostolova LG, Green AE, Avedissian C, Madsen SK, et al. Automated 3D mapping of hippocampal atrophy and its clinical correlates in 400 subjects with Alzheimer's disease, mild cognitive impairment, and elderly controls. *Hum Brain Mapp* 2009a; 30: 2766–88.
- Morra JH, Tu Z, Apostolova LG, Green AE, Avedissian C, Madsen SK, et al. Automated mapping of hippocampal atrophy in 1-year repeat MRI data from 490 subjects with Alzheimer's disease, mild cognitive impairment, and elderly controls. *NeuroImage* 2009b; 45 (1 Suppl): S3–15.
- Morris JC. The Clinical Dementia Rating (CDR): current version and scoring rules. *Neurology* 1993; 43: 2412–4.
- Morris JC, Roe CM, Grant EA, Head D, Storandt M, Goate AM, et al. Pittsburgh compound b imaging and prediction of progression from cognitive normality to symptomatic Alzheimer disease. *Arch Neurol* 2009; 66: 1469–75.
- Nordberg A. Amyloid imaging in Alzheimer's disease. *Curr Opin Neurol* 2007; 20: 398–402.
- Nordberg A. Amyloid plaque imaging in vivo: current achievement and future prospects. *Eur J Nucl Med Mol Imaging* 2008; 35 (Suppl 1): S46–50.
- Palop JJ, Mucke L. Epilepsy and cognitive impairments in Alzheimer disease. *Arch Neurol* 2009; 66: 435–40.
- Petersen RC, Aisen PS, Beckett LA, Donohue MC, Gamst AC, Harvey DJ, et al. Alzheimer's Disease Neuroimaging Initiative (ADNI): clinical characterization. *Neurology* 2010; 74: 201–9.
- Petersen RC, Roberts RO, Knopman DS, Boeve BF, Geda YE, Ivnik RJ, et al. Mild cognitive impairment: ten years later. *Arch Neurol* 2009; 66: 1447–55.
- Pike KE, Savage G, Villemagne VL, Ng S, Moss SA, Maruff P, et al. β -amyloid imaging and memory in non-demented individuals: evidence for preclinical Alzheimer's disease. *Brain* 2007; 130: 2837–44.
- Price JC, Klunk WE, Lopresti BJ, Lu X, Hoge JA, Ziolkowski SK, et al. Kinetic modeling of amyloid binding in humans using PET imaging and Pittsburgh Compound-B. *J Cereb Blood Flow Metab* 2005; 25: 1528–47.
- Rowe CC, Ng S, Ackermann U, Gong SJ, Pike K, Savage G, et al. Imaging β -amyloid burden in aging and dementia. *Neurology* 2007; 68: 1718–25.
- Schroeter ML, Stein T, Maslowski N, Neumann J. Neural correlates of Alzheimer's disease and mild cognitive impairment: a systematic and quantitative meta-analysis involving 1351 patients. *NeuroImage* 2009; 47: 1196–206.
- Shattuck DW, Leahy RM. BrainSuite: an automated cortical surface identification tool. *Med Image Anal* 2002; 6: 129–42.
- Sperling RA, LaViolette PS, O'Keefe K, O'Brien J, Rentz DM, Pihlajamaki M, et al. Amyloid deposition is associated with impaired default network function in older persons without dementia. *Neuron* 2009; 63: 178–88.

- Stoub TR, Bulgakova M, Leurgans S, Bennett DA, Fleischman D, Turner DA, et al. MRI predictors of risk of incident Alzheimer disease: a longitudinal study. *Neurology* 2005; 64: 1520–4.
- Thompson PM, Hayashi KM, de Zubicaray G, Janke AL, Rose SE, Semple J, et al. Dynamics of grey matter loss in Alzheimer's disease. *J Neurosci* 2003; 23: 994–1005.
- Thompson PM, Hayashi KM, de Zubicaray GI, Janke AL, Rose SE, Semple J, et al. Mapping hippocampal and ventricular change in Alzheimer disease. *NeuroImage* 2004; 22: 1754–66.
- Tolboom N, van der Flier WM, Yaquib M, Boellaard R, Verwey NA, Blankenstein MA, et al. Relationship of cerebrospinal fluid markers to 11C-PiB and 18F-FDDNP binding. *J Nucl Med* 2009a; 50: 1464–70.
- Tolboom N, Yaquib M, van der Flier WM, Boellaard R, Luurtsema G, Windhorst AD, et al. Detection of Alzheimer pathology in vivo using both 11C-PiB and 18F-FDDNP PET. *J Nucl Med* 2009b; 50: 191–7.
- Tosun D, Schuff N, Truran-Sacrey D, Shaw LM, Trojanowski JQ, Aisen P, et al. Relations between brain tissue loss, CSF biomarkers, and the ApoE genetic profile: a longitudinal MRI study. *Neurobiol Aging* 2010; 31: 1340–54.
- Villemagne V, Fodero-Tavoletti M, Pike K, Cappai R, Masters C, Rowe C. The ART of loss: A β Imaging in the evaluation of Alzheimer's disease and other dementias. *Mol Neurobiol* 2008; 38: 1–15.
- Wechsler D. Wechsler Memory Scale-Revised (WMS-R). New York: Psychological Corporation; 1987.
- Whitwell JL, Przybelski SA, Weigand SD, Knopman DS, Boeve BF, Petersen RC, et al. 3D maps from multiple MRI illustrate changing atrophy patterns as subjects progress from mild cognitive impairment to Alzheimer's disease. *Brain* 2007; 130: 1777–86.
- Whitwell JL, Shiung MM, Przybelski SA, Weigand SD, Knopman DS, Boeve BF, et al. MRI patterns of atrophy associated with progression to Alzheimer's disease in amnesic mild cognitive impairment. *Neurology* 2008; 70: 512–20.
- Wilson AA, Garcia A, Chestakova A, Kung H, Houle S. A rapid one-step radiosynthesis of the beta-amyloid imaging radiotracer N-methyl-11C 2-(4prime-methylaminophenyl)-6-hydroxybenzothiazole (11C-6-OH-BTA-1). *J Labelled Comp Radiopharm* 2004; 47: 679–82.
- Woods RP, Mazziotta JC, Cherry SR. MRI-PET registration with automated algorithm. *J Comp Assist Tomogr* 1993; 17: 536–46.
- Worsley KJ, Taylor JE, Tomaiuolo F, Lerch J. Unified univariate and multivariate random field theory. *NeuroImage* 2004; 23 (Suppl 1): S189–95.
- Yvette IS, Marcus ER, Abraham ZS, John CM, Denise H, Suzhi W, et al. Amyloid plaques disrupt resting state default mode network connectivity in cognitively normal elderly. *Biol Psychiatry* 2010; 67: 584–7.
- Zhou J, Greicius MD, Gennatas ED, Growdon ME, Jang JY, Rabinovici GD, et al. Divergent network connectivity changes in behavioural variant frontotemporal dementia and Alzheimer's disease. *Brain* 2010; 133: 1352–67.